

# Northumbria Research Link

Citation: Chen, Fei, Guo, Changxiang, Zhou, Honghao, Shahzad, Muhammad Wakil, Liu, Xiaoteng, Oleksandr, Sokolskyi, Dai, Sheng and Xu, Bin (2022) Supramolecular Network Structured Gel Polymer Electrolyte with High Ionic Conductivity for Lithium Metal Batteries. *Small*, 18 (43). p. 2106352. ISSN 1613-6810

Published by: Wiley-Blackwell

URL: <https://doi.org/10.1002/sml.202106352> <<https://doi.org/10.1002/sml.202106352>>

This version was downloaded from Northumbria Research Link:  
<https://nrl.northumbria.ac.uk/id/eprint/47990/>

Northumbria University has developed Northumbria Research Link (NRL) to enable users to access the University's research output. Copyright © and moral rights for items on NRL are retained by the individual author(s) and/or other copyright owners. Single copies of full items can be reproduced, displayed or performed, and given to third parties in any format or medium for personal research or study, educational, or not-for-profit purposes without prior permission or charge, provided the authors, title and full bibliographic details are given, as well as a hyperlink and/or URL to the original metadata page. The content must not be changed in any way. Full items must not be sold commercially in any format or medium without formal permission of the copyright holder. The full policy is available online: <http://nrl.northumbria.ac.uk/policies.html>

This document may differ from the final, published version of the research and has been made available online in accordance with publisher policies. To read and/or cite from the published version of the research, please visit the publisher's website (a subscription may be required.)

1  
2  
3  
4  
5  
6  
7  
8  
9  
10  
11  
12  
13  
14  
15  
16  
17  
18  
19  
20  
21  
22  
23  
24  
25  
26  
27  
28  
29  
30  
31  
32  
33

## **Supramolecular Network Structured Gel Polymer Electrolyte with High Ionic Conductivity for Lithium Metal Batteries**

*Fei Chen,\* Changxiang Guo, Honghao Zhou, Muhammad Wakil Shahzad, Terence Xiaoteng Liu, Sokolskyi Oleksandr, Jining Sun, Sheng Dai and Ben Bin Xu\**

F. Chen, C. Guo  
Shaanxi Key Laboratory of Energy Chemical Process Intensification, School of Chemical Engineering and Technology, Xi'an Jiaotong University, Xi'an, Shaanxi, 710049, PR China  
E-mail: feichen@xjtu.edu.cn

H. Zhou, M. Shahzad, T. Liu, B. Xu  
Mechanical and Construction Engineering, Faculty of Engineering and Environment, Northumbria University, Newcastle upon Tyne, NE1 8ST, UK  
E-mail: ben.xu@northumbria.ac.uk

S. Oleksandr  
Department of Chemical, Polymer and Silicate Engineering, Igor Sikorsky Kyiv Polytechnic Institute, Kyiv, 03056, Ukraine

J. Sun  
School of Mechanical Engineering, Dalian University of Technology, Dalian, China, 116024

S. Dai  
Department of Chemical Engineering, Brunel University London, Uxbridge UB8 2DW, UK

Keywords: supramolecular network, lithium metal batteries, ionic conductivity, high-voltage electrolyte, GPEs

1 **Abstract**

2 Polymer-based solid electrolytes (PSEs) offer great promises in developing lithium metal  
3 batteries due to their attractive features such as safety, lightweight, low cost and high  
4 processability. However, PSE-based lithium battery usually requires a relatively high  
5 temperature (60 °C or above) to complete charge and discharge due to the poor ionic  
6 conductivity of PSEs. Herein, we design and develop a Gel polymer electrolytes (GPEs) film  
7 with a supramolecular network structure through a facile one-step photopolymerization. The  
8 crosslinked structure and quadruple hydrogen bonding fulfil the GPEs with high thermal  
9 stability and good mechanical property with a maximum tensile strain of 48 %. The obtained  
10 GPEs possess a high ionic conductivity of  $3.8 \times 10^{-3} \text{ S cm}^{-1}$  at 25 °C and a decomposition voltage  
11  $\geq 4.6 \text{ V}$  (vs. Li/Li<sup>+</sup>). The cells assembled with LiFePO<sub>4</sub> (LFP) cathode and Li anode, present an  
12 initial discharge specific capacity of 155.6 mAh g<sup>-1</sup> and a good cycling efficiency with a  
13 capacity retention rate of 81.1% after 100 charges/discharge cycles at 0.1C at ambient  
14 temperature. This work encompasses a new route to develop high performance PSEs that can  
15 be operated at room temperature for future lithium metal batteries.

16

17

## 1 1. Introduction

2           Operational safety has drawn considerable attention for lithium-ion (Li-ion) batteries,  
3 where the replacement of flammable liquid electrolytes with solid electrolytes appears to be a  
4 sensible choice.<sup>[1]</sup> Besides, the solid-state electrolyte is featured for higher energy density to  
5 benefit future Li-ion batteries.<sup>[2]</sup> Lithium metal anode ( $3860 \text{ mAh g}^{-1}$ ) has a higher theoretical  
6 specific capacity and lower electrochemical potential ( $-3.04 \text{ V vs. hydrogen potential}$ ) than  
7 graphite anode ( $372 \text{ mAh g}^{-1}$ ), and replacing graphite anode ( $250 \text{ Wh Kg}^{-1}$ ) with lithium metal  
8 anode ( $440 \text{ Wh Kg}^{-1}$ ) can double the effective energy for battery.<sup>[3]</sup> However, the lithium  
9 dendrite on the anode can trigger the diaphragm to fracture during the operation, the resulting  
10 short-circuit in battery ultimately lead to fire and losses of life or property.<sup>[4]</sup> The replacement  
11 of diaphragm by solid-state electrolytes dramatically simplifies the battery production process  
12 and greatly enhances the safety. Polymer solid-state electrolyte (PSE) has emerged to lead solid-  
13 state electrolyte technology for its simple production, molecular modifiability, low cost and  
14 good processability.<sup>[5]</sup> However, the low ionic conductivity of PSEs seriously hinders their  
15 applications.<sup>[6]</sup>

16           To increase the ionic conductivity of PSEs, researchers have made a variety of attempts,  
17 for example, replacing lithium salts with different anions, adding plasticizers, preparing  
18 composite polymer electrolytes, etc. Polyethylene oxide (PEO) has been known as a promising  
19 candidate for PSEs, for its unique capability to dissolve lithium ions. But the high crystallinity  
20 of PEO at room temperature leads to a low ionic conductivity ( $10^{-8}\sim 10^{-5} \text{ S cm}^{-1}$ ), therefore its  
21 actual operating temperature needs to be  $60 \text{ }^\circ\text{C}$  or above.<sup>[7]</sup> Notably, Wang and co-workers have  
22 managed to increase the ionic conductivity of polymer electrolyte to  $1.1\times 10^{-4} \text{ S cm}^{-1}$  at  $35 \text{ }^\circ\text{C}$   
23 by reducing the crystallinity of PEO and the Li/PEO-HPMA/LFP cell can maintain a reversible  
24 capacity of  $80.4 \text{ mAh g}^{-1}$  at 1C rate.<sup>[8]</sup> Wan *et al* mixed PEO and  $\text{Li}_7\text{La}_3\text{Zr}_2\text{O}_{12}$  to produce a  
25 composite solid-state electrolyte film with improved ionic conductivity to obtain specific

1 capacity 158.7 mAh g<sup>-1</sup> at 0.1 C in LFP/PLLN/Li batteries, with an operational temperature  
2 below 45 °C.<sup>[9]</sup> Bouchet and co-workers prepared a single-ion conductor triblock copolymer  
3 P(STFSiLi)-*b*-PEO-*b*-P(STFSiLi) based LFP/Li with a discharge specific capacity of 160 mAh  
4 g<sup>-1</sup> at C/8 under 80 °C.<sup>[10]</sup> Feng and co-workers developed a single Li-ion polymer electrolyte  
5 approach with utilizing P(SSPSiLi-*alt*-MA) as the active ingredient and realized single LFP/Li  
6 battery with a specific capacity higher than 150 mAh g<sup>-1</sup> at 0.02C under 80 °C.<sup>[11]</sup> Xue *et al*  
7 synthesized a cross-linked polymer solid-state electrolyte, CPSHPE, with a good flame  
8 retardancy, self-healing capability and an initial discharge capacity of 130 mAh g<sup>-1</sup> at 0.1C  
9 below 60 °C with LFP/Li cells.<sup>[12]</sup> Although ionic conductivity can be significantly enhanced  
10 using above approaches, high operational temperature of charge/discharge cycles still remains  
11 as a challenge in exploring solid-state electrolyte applications in lithium metal batteries.

12 Gel polymer electrolyte (GPE), a supramolecular network structured polymer  
13 electrolyte, hold more potentials for commercialisation than other PSEs, with high ionic  
14 conductivity and superior electrode/electrolyte interfacial properties, excellent mechanical  
15 properties (strength, flexibility, etc.) and enhanced safety. Cross-linked polymers offer many  
16 advantages in achieving mechanically robust polymer electrolyte, including easy synthesis, the  
17 ability to suppress the crystallinity of polymer, and increased polymer mechanical strength.<sup>[13]</sup>  
18 Here, we propose a supramolecular network structured polymer electrolyte approach to achieve  
19 good mechanical properties and high ionic conductivity electrolytes. The poly(ethylene glycol)  
20 methyl ether methacrylate (PEGMA), 2-(3-(6-methyl-4-oxo-1,4-dihydropyrimidin-2-  
21 yl)ureido)ethyl methacrylate (UPyMA) tripropylene glycol diacrylate (TPGDA) and 1-Allyl-3-  
22 methylimidazolium Bis(trifluoromethanesulfonyl)imide (AMIMTFSI) will form the skeleton  
23 of polymer electrolyte, with UPyMA in the cross-linked structure to provide better mechanical  
24 strength since their dimers will form a quadruple hydrogen bonding interaction. The  
25 supramolecular gel network also contains small residual molecules such as ionic liquid (IL)  
26 monomers and prepolymers that have not undergone polymerisation, thus providing a high

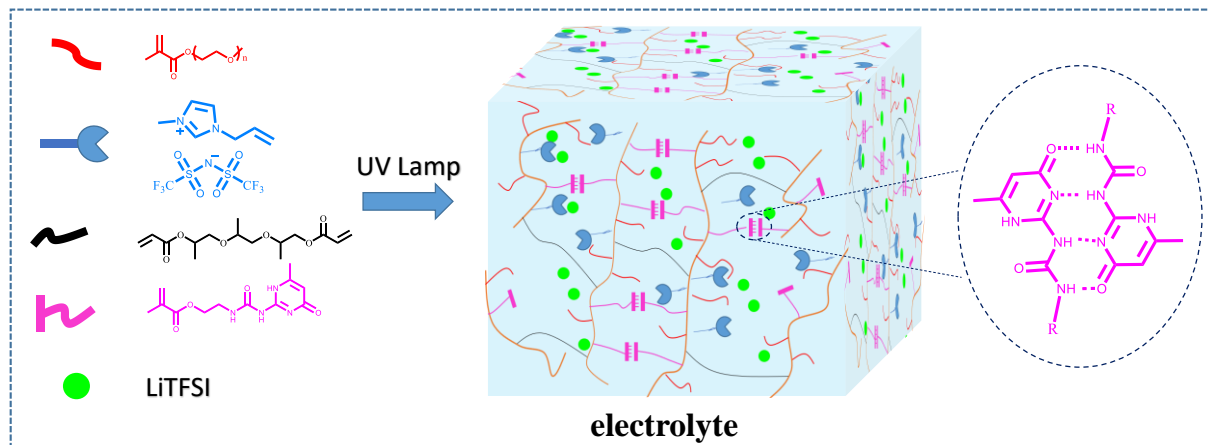
1 ionic conductivity. Furthermore, the GPEs developed in this paper have been assembled in  
 2 lithium metal batteries and have been tested with good charge/discharge cycle capability at  
 3 room temperature (25 °C).

4

## 5 2. Results and Discussion

### 6 2.1. Design and Preparation of PUTP Electrolytes

7 The supramolecular network structured gel is photo-synthesized (**Figure 1**). In the  
 8 supramolecular network structure, PEGMA and AMIMTFSI not only provide the polymeric  
 9 substrate but also effectively influence the transport of ions. Meanwhile, the quadruple  
 10 hydrogen bonding networks constructed by the interaction of UPyMA dimers give the polymer  
 11 electrolyte good mechanical performance. Table 1 shows the monomers proportions, the glass  
 12 transition temperature and ionic conductivity of PUTP GPE samples.



13

14 **Figure 1.** Schematic illustration of the monomers and one-step photosynthesis of PUTP GPEs.

15

16 Fourier-transform infrared spectra (FTIR) were employed to verify the polymerization  
 17 of monomers. The FTIR spectra clearly show the chemical structure of UPyMA, PEGMA,  
 18 TPGDA, AMIMTFSI, PUTP1, PUTP2, and PUTP3 (Figure S1-S7). For the monomers of  
 19 AMIMTFSI, UPyMA, the characteristic peaks stretching bands of C=C at 1650  $\text{cm}^{-1}$ . PEGMA

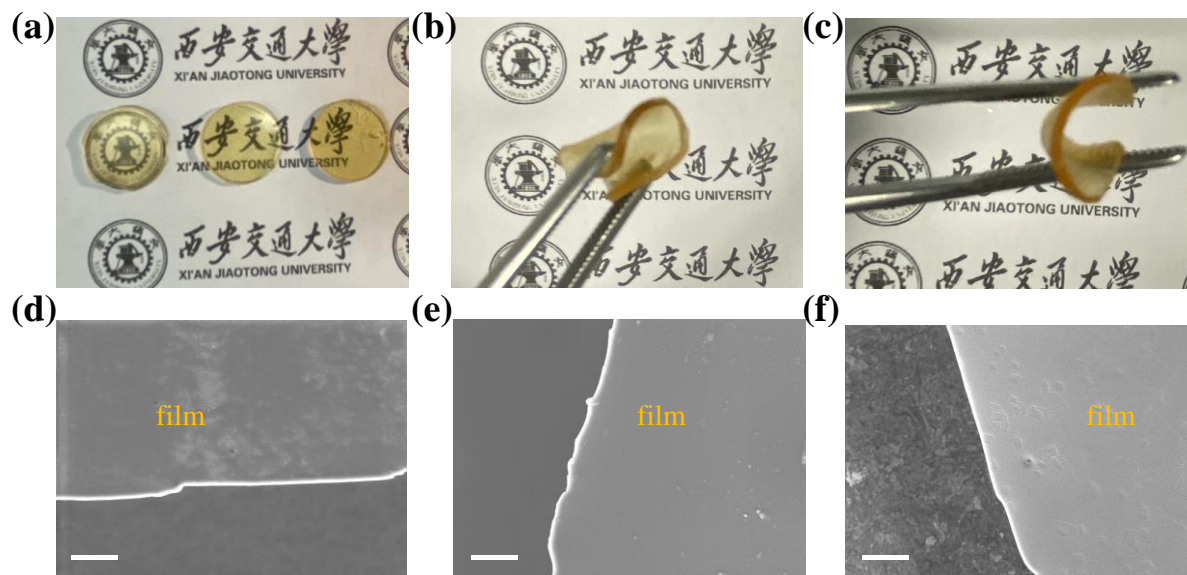
1 and TPGDA, the stretching bands of C=C and C=O give their characteristic peaks at 1638 cm<sup>-1</sup>  
 2 and 1726 cm<sup>-1</sup>. After polymerization, the C=C stretching vibrations no disappear in PUTP1,  
 3 PUTP2, and PUTP3 samples, demonstrating that the polymerization is not fully completed  
 4 under the initiation of UV light. These monomers or prepolymers, which do not polymerise, are  
 5 existing in the supramolecular network in a free form, thus forming ion transport channels with  
 6 the PEG/PIL chains in the crosslinked network. For the PUTP, four characteristic absorption  
 7 peaks of the TFSI anion can be observed in the spectrum at 1060 cm<sup>-1</sup>, 1138 cm<sup>-1</sup>, 1196 cm<sup>-1</sup>  
 8 and 1350 cm<sup>-1</sup>, indicating that the TFSI is successfully dispersed in the network.

10 **Table 1** Molar ratio of PEGMA to UPyMA,  $T_g$  and ionic conductivity of PUTP electrolyte

Electrolyte	PEGMA:UPyMA (by mole)	$T_g$ °C	$\sigma$ at 25 °C S cm <sup>-1</sup>
PUTP1	10:1	-62.7	$3.8 \times 10^{-3}$
PUTP2	5:1	-62.2	$2.8 \times 10^{-3}$
PUTP3	2.5:1	-61.6	$2.5 \times 10^{-3}$

11  
 12 The PUTP electrolyte system contains a cross-linked supramolecular network formed  
 13 by TPGDA as a cross-linking agent and UPyMA quadruple hydrogen bonding. **Figure 2a** shows  
 14 the optical photographs for PUTP1, PUTP2, and PUTP3 samples, respectively. The elasticity  
 15 (flexibility) of solid electrolyte is demonstrated by folding PUTP1 in a different direction  
 16 (Figure 2b and 2c), where the film can be folded and don't break. The flexible nature of  
 17 polymeric solid electrolytes offers a great advantage to be applied in flexible electronic devices.  
 18 The scanning electron microscopy (SEM) observations show a uniform and flat surface of  
 19 PUTP solid electrolyte. The SEM images of PUTP1, PUTP2, and PUTP3 samples are shown  
 20 in Figure 2d-2f. This interface ensured good contact between the electrolyte and positive/

1 negative electrodes in the cell. As shown in Figure S8-S10, the detailed elemental distribution  
2 scanning (EDS) results present the uniform distribution of C, N, O, F, and S elements, indicating  
3 a uniform distribution of LiTFSI in the PUTP electrolyte.



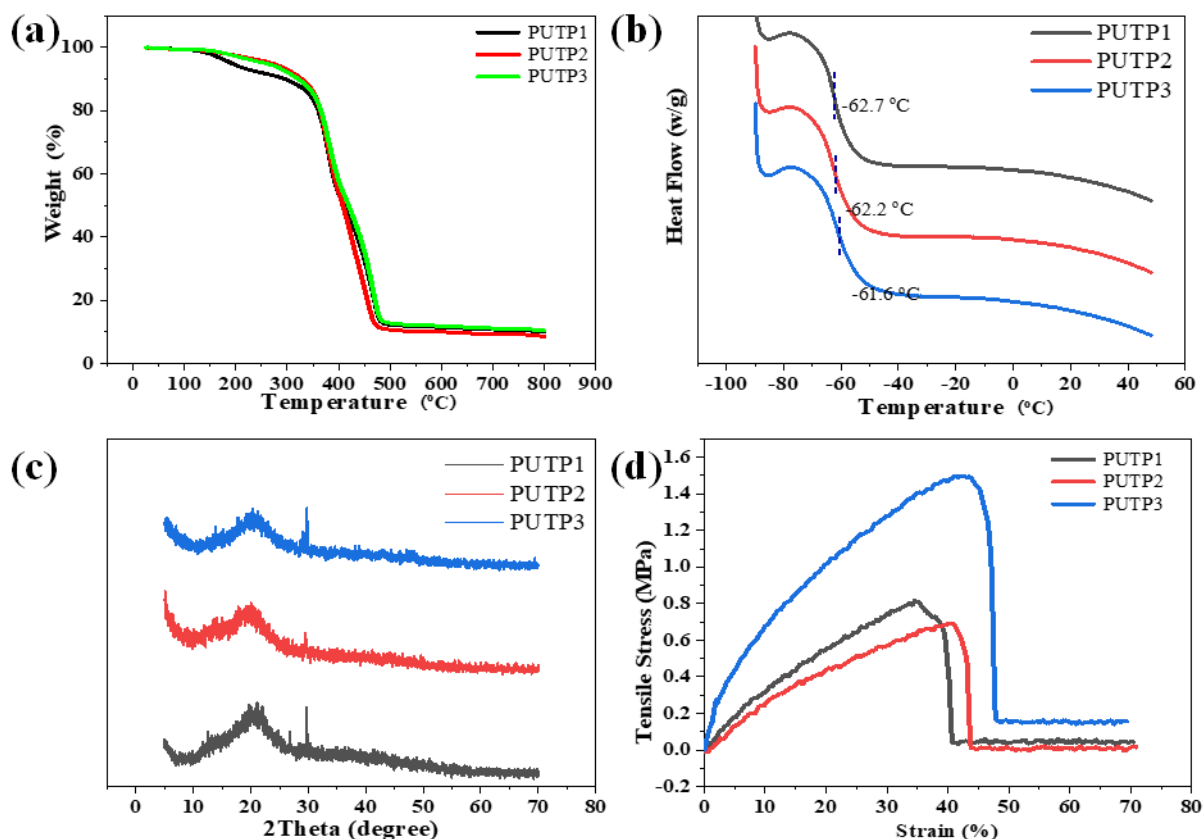
4  
5 **Figure 2.** (a). Optical images (from left to right) of PUTP1, PUTP2, and PUTP3. (b) Photograph  
6 of PUTP1 electrolyte folded from the front with tweezers. (c) Photograph of PUTP1 electrolyte  
7 folded from the back with tweezers. Scanning electron micrographs of d) PUTP1, e) PUTP2  
8 and f) PUTP3. Scale bars: 20 μm.

9

## 10 2.2. Physical Properties of Electrolytes

11 The thermal stability of PSEs is of vital importance to the safety of lithium metal  
12 batteries. Thermal gravimetric analysis (TGA) was conducted on three obtained electrolyte  
13 samples to investigate the effect of UPyMA on the thermal decomposition temperature. As  
14 shown in **Figure 3a**, the thermal decomposition curves of PUTP1, PUTP2, and PUTP3 showed  
15 their decomposition temperatures at 192 °C, 270 °C and 270 °C respectively. The decomposition  
16 temperatures of all polymer electrolytes are higher than the melting point of lithium metal (180  
17 °C), confidently proving that these electrolytes can perform their duty safely in lithium metal  
18 batteries with qualified thermal stability.





1  
 2 **Figure 3.** (a) TGA curves of PUTP1, PUTP2, and PUTP3 performed under inert N<sub>2</sub>. (b) DSC  
 3 curves of PUTP1, PUTP2, and PUTP3 were performed at -90-50 °C. (c) XRD curves of PUTP1,  
 4 PUTP2, and PUTP3 were conducted at 5-70. (d) The stress-strain curve of PUTP1, PUTP2, and  
 5 PUTP3, for which the parameters of the process in the test were set to a tensile rate of 10 mm  
 6 min<sup>-1</sup> and a sample size of 20 × 5 × 0.2 mm<sup>3</sup>.

7  
 8 The differential scanning calorimetry (DSC) results (Figure 3b) reveal  $T_g$  values as -  
 9 62.7 °C, -62.2 °C and -61.6 °C for PUTP1, PUTP2, and PUTP3 electrolytes, respectively.  
 10 Furthermore, the  $T_g$  of PUTP1, PUTP2, and PUTP3 electrolytes have been found to increase  
 11 with the increase of UPyMA content. The crystalline properties of three samples were examined  
 12 by X-ray Diffraction (XRD). There are no significant crystalline peaks from the XRD curves  
 13 (Figure 3c), suggesting that all three polymeric solid electrolytes are in an amorphous form.  
 14 The tensile testing results in Figure 3d demonstrate that, as UPyMA content increases, the  
 15 maximum tensile strains of PUTP1, PUTP2, and PUTP3 electrolytes gradually increase, with  
 16 PUTP3 having superior mechanical tensile properties with 48 % maximum tensile strain. Apart

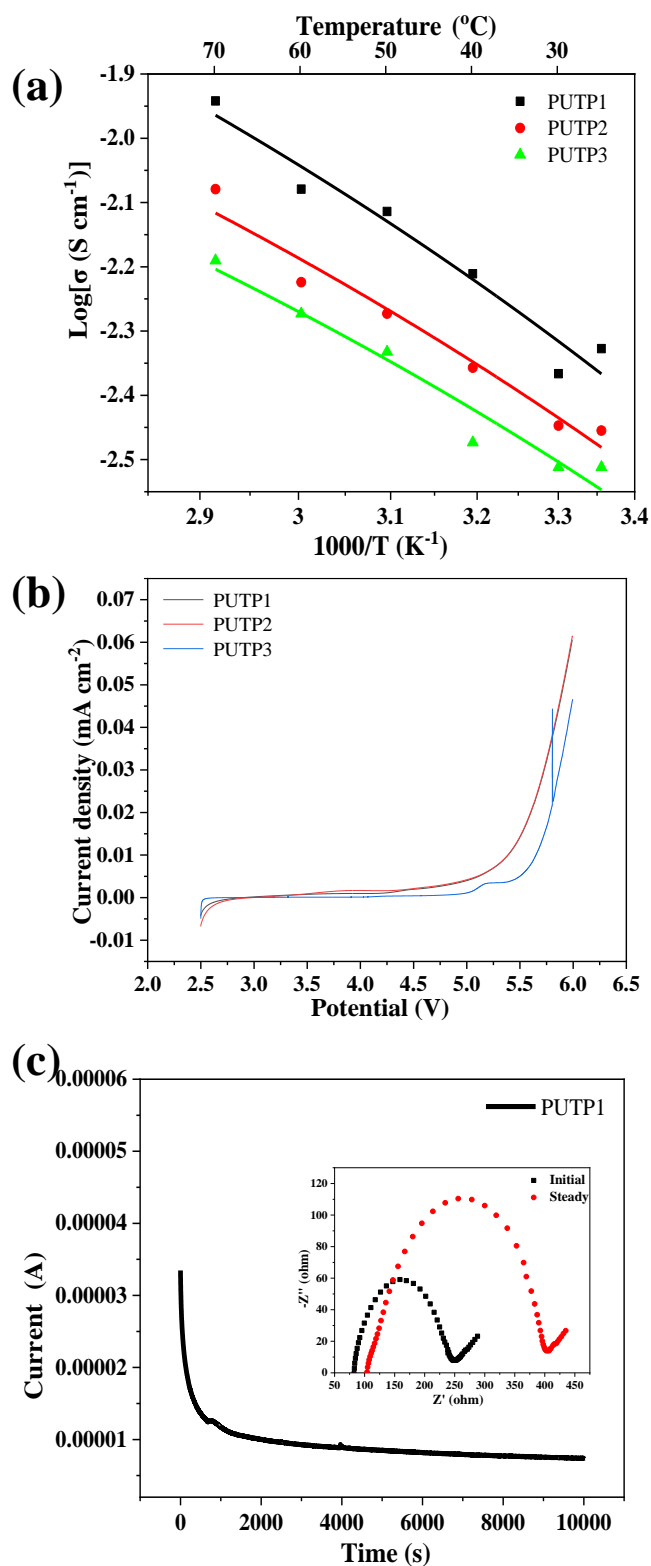
1 from the chemical cross-linking, the physical cross-linking induced by the quadruple hydrogen  
2 bonding of UPyMA dimer also contributes to the mechanical enhancement of electrolytes.

3

### 4 **2.3. Electrochemical Performance**

5 In addition to the mechanical properties, the polymer electrolyte needs to reach several  
6 electrochemical merits to achieve a quality charging and discharging performance. The ionic  
7 conductivity, decomposition voltage, and lithium-ion transference number are three top  
8 electrochemical parameters for PSEs. First, AC impedance spectra were used to characterize  
9 the ionic conductivity of PUTP1, PUTP2 and PUTP3 (Figure S11-S13). The ionic conductivity  
10 of three electrolytes (**Figure 4a**) is calculated by Equation 1 as a function of temperature from  
11 25 °C to 70 °C. The ionic conductivity gradually increases when temperature elevates, it is found  
12 that the ionic conductivity with temperature conforms to the VTF equation by fitting the  
13 conductivity curve. It is found that PUTP1 has the highest ionic conductivity of  $3.8 \times 10^{-3} \text{ S cm}^{-1}$   
14 at 25 °C. The ionic conductivity of PUTP2 and PUTP3 are  $2.8 \times 10^{-3}$  and  $2.5 \times 10^{-3} \text{ S cm}^{-1}$  at 25  
15 °C, respectively.

16



1  
 2 **Figure 4.** (a) Temperature-dependent ionic conductivity of PUTP1, PUTP2, and PUTP3 thin-  
 3 film electrolytes. (b) LSV curves of PUTP1, PUTP2, and PUTP3 thin-film electrolytes (c)  
 4 Chronoamperometry profile of Li/PUTP1/Li cells at 25  $^{\circ}\text{C}$  and the inset shows the impedance  
 5 spectra before and after chronoamperometry.

1           The electrochemical stability of polymer electrolyte is particularly important from the  
2 operational safety perspective, which requires the electrolyte not to decompose or undergo  
3 electrochemical reactions within the battery charging and discharging voltage range. The anodic  
4 limiting potentials of PUTP1, PUTP2 and PUTP3 were measured by linear scanning  
5 voltammetry (LSV) for Li/PUTP/stainless cells at 25 °C with LSV measurements in the voltage  
6 range 2.5 V - 6 V vs. Li/Li<sup>+</sup> at a scan rate of 1 mV s<sup>-1</sup>. In Figure 4b, the LSV curves show a  
7 steady current plateau until 4.6 V, suggesting a high decomposition voltage above 4.6 V for all  
8 solid electrolytes. When the voltage exceeds 4.6 V, the current increases, indicating that the  
9 electrolyte starts to decompose. The wide electrochemical stability shows excellent  
10 electrochemical stability that could satisfy the requirements for a high voltage battery. As shown  
11 in Figure 4c, the calculated  $t_{\text{Li}^+}$  (calculated by the Bruce-Vincent equation, Equation 2) for  
12 PUTP1, PUTP2 and PUTP3 are 0.13, 0.12 and 0.17, respectively. The low Li-ion transference  
13 number is caused by the existence of a significant number of freely flowing TFSI negative ions  
14 and mobile AMIM<sup>+</sup> cations in the electrolyte system. The constant potential polarization curves  
15 and AC impedance spectra of PUTP2 and PUTP3 are shown in Figures S14 and S15.

16

## 17 **2.4. Battery Performance**

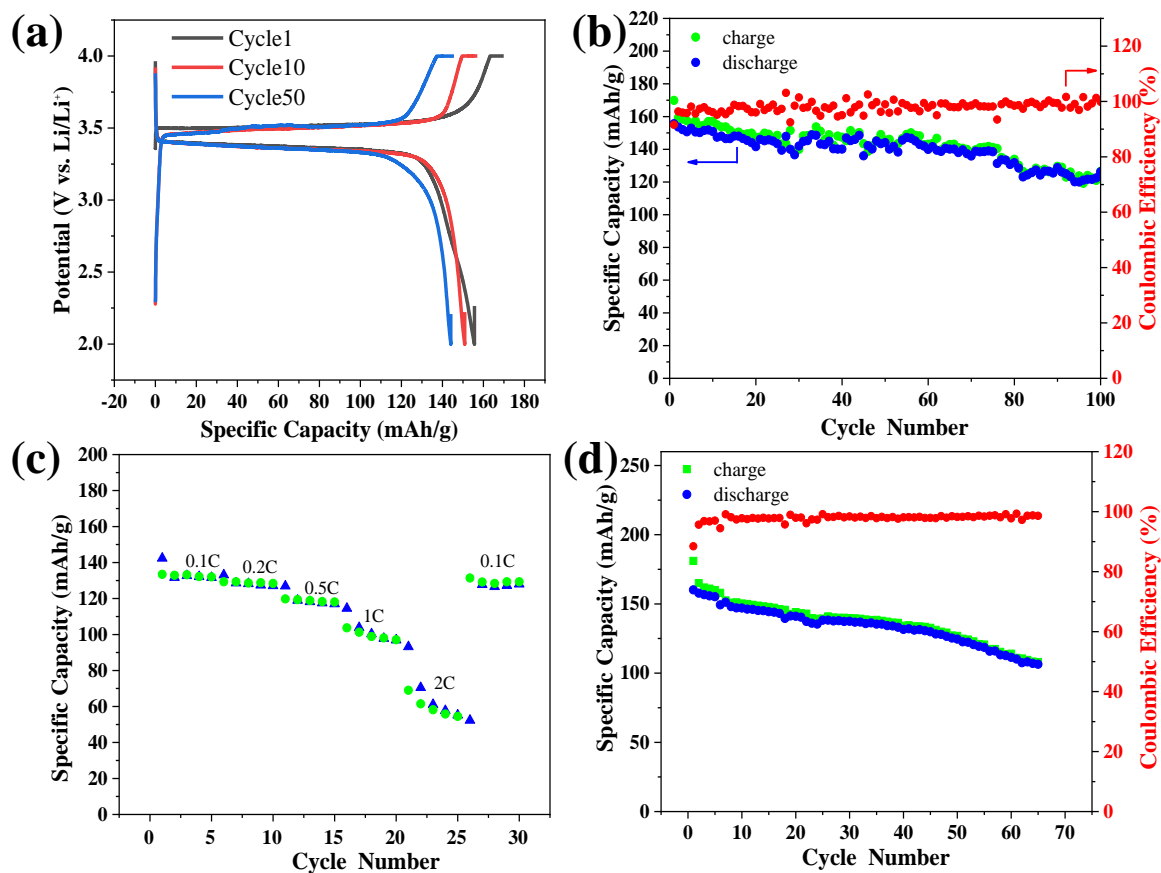
18           The battery performance of obtained GPEs are measured at room temperature and 25  
19 °C. As shown in Figure S16, the PUTP1 electrolyte exhibits a small overpotential in the  
20 Li/PUTP1/Li symmetric cell with an overpotential of 30 mV at a current density of 0.05 mA  
21 cm<sup>-2</sup> and 75 mV at a current density of 0.1 mA cm<sup>-2</sup>. The overpotential of the symmetric cell at  
22 cycling at different current densities showed an increase in voltage polarization along with the  
23 increment in current density. Interestingly, the overpotential remained approximately stable at  
24 the same current density, indicating that the electrolyte has good compatibility with lithium

1 metal.<sup>[15]</sup> Moreover, the symmetric cells do not show a short circuit after cycling for 400 hours,  
2 indicating a strong reliability. The Li/PUTP2/Li symmetric cell and the Li/PUTP3/Li symmetric  
3 cell both have a small overpotential and no short circuit after cycling (Figure S17 and S18).

4 The cyclic voltammetry curve of Li/PUTP1/LFP cell is shown in Figure S19, with 10  
5 cycles in the voltage range of 2.5 V - 4 V and a scan rate of 0.1 mV s<sup>-1</sup>. The oxidation peak at  
6 3.69 V represents the process of lithium-ion detachment from LFP, while the reduction peak at  
7 3.17 V represents the process of lithium-ion embedding into LFP. After the first cycle is  
8 completed, the pair of redox peaks remains essentially unchanged, suggesting significant  
9 stability between the LFP cathode and the PUTP electrolyte. Additionally, the cyclic  
10 voltammetry curves of the Li/PUTP2/LFP cell and the Li/PUTP3/LFP cell are shown in Figures  
11 S20 and S21.

12 The charge/discharge voltage curves of the Li/PUTP1/LFP battery at 0.1C at a room  
13 temperature are clearly shown in **Figure 5a**, with the charge plateau at 3.49 V and the discharge  
14 plateau at 3.38 V. The difference value in charge and discharge voltage plateaus is 110 mV,  
15 which is compatible with asymmetric battery's lower polarization voltage. The charging and  
16 discharging plateaus are symmetrical, meaning that the electrochemical reactions that occur  
17 while charging and discharging in the cell are reversible.<sup>[16]</sup> In addition, Figure 5b shows that  
18 the lithium battery based on PUTP1 electrolyte can be better charged and discharged for at least  
19 100 cycles at room temperature at 0.1C, and the Coulomb efficiency can reach more than 96%,  
20 and the initial discharge specific capacity of the battery is 155.6 mAh g<sup>-1</sup>, and the discharge  
21 specific capacity remains at 126.2 mAh g<sup>-1</sup> after 100 cycles, with a capacity retention rate of  
22 81.1%.

23



1  
2 **Figure 5.** (a) Voltage curves of Li/PUTP1/LFP battery charged and discharged at a current rate  
3 of 0.1 C at room temperature for the first, tenth and fiftieth cycles. (b) Galvanostatic charge-  
4 discharge profiles of Li/PUTP1/LFP for 100 cycles at 0.1C at room temperature. (c) The rate  
5 capability of Li/PUTP1/LFP cell at 25 °C. (d) Graphs of specific capacity and Coulombic  
6 efficiency at 0.2 C at 25 °C of PUTP1 base battery.

7  
8 The rate performance of the Li/PUTP1/LFP battery is shown in Figure 5c. The discharge  
9 specific capacity of battery at rate of 0.1C, 0.2C, 0.5C, 1C, 2C, and 0.1C are 133.4, 129.3, 119.8,  
10 103.7, 69.0, and 131.4 mAh g<sup>-1</sup>, respectively. The results of cell rate tests show that the PUTP1  
11 electrolyte has a good rate performance. Li/PUTP2/LFP and Li/PUTP3/LFP cells rate  
12 performance are shown in (Figure S22 and S23). Compared to PUTP1, PUTP2 and PUTP3  
13 exhibit poor rate performance. Even though UPyMA can enhance the mechanical properties of  
14 electrolyte through quadruple hydrogen bonding, the rate capability performance deteriorates  
15 with increasing UPyMA. The three supramolecular gel polymer electrolytes PUTP1, PUTP2,

1 and PUTP3 have a progressive increase in the proportion of UPyMA monomers, which  
2 increases the likelihood that UPyMA will be present on the surface of the electrolyte in higher  
3 amounts. Excessive UPyMA on the surface may lead to poor wettability between electrolyte  
4 and electrode, resulting in differences in rate capability. Figure 5d shows the charge/discharge  
5 cycling performance of the PUTP1 electrolyte at 0.2C at 25 °C. The Li/PUTP1/LFP coin cell  
6 was first assembled and activated by five charge/discharge cycles at 0.1C, followed by 60 cycles  
7 at 0.2C with an initial discharge specific capacity of 149.3 mAh g<sup>-1</sup>. After 60 cycles, the specific  
8 capacity decays at a rate of 0.71 mAh g<sup>-1</sup> per cycle, but still maintains a specific capacity of  
9 106.4 mAh g<sup>-1</sup>. In the supporting material, the charge/discharge cycles of a Li/PUTP2/LFP coin  
10 cell and a Li/PUTP3/LFP coin cell with 0.2C are shown (Figure S24 and S25). The specific  
11 capacity of Li/PUTP3/LFP at 0.2C decays from 101.1 mAh g<sup>-1</sup> at the beginning to 48.0 mAh g<sup>-1</sup>  
12 after 60 cycles, which may be attributed to the increase in UPyMA content, which makes the  
13 electrolyte more likely to form dimers under prolonged operating conditions.

14

### 15 3. Conclusion

16 In summary, we describe a facile one-step UV light polymerization strategy to achieve  
17 supramolecular network GPEs. The mechanical properties of synthesized solid electrolytes are  
18 improved with the increase of UPyMA content (stretching rate ~ 48% for PUTP3), while  
19 PUTP1 shows the highest ionic conductivity at 25 °C ( $3.8 \times 10^{-3}$  S cm<sup>-1</sup>). In addition, the GPEs  
20 in this paper not only have good mechanical strength but also possess high ionic conductivity.  
21 High ionic conductivity of GPEs is attributed to the ion transport by multiple ion channels in  
22 the supramolecular network structure, while the good mechanical properties of GPEs is due to  
23 the supramolecular network structure of UPyMA dimer. After assembling the solid-state  
24 electrolyte into a symmetric Li/PUTP/Li battery, it is found that the solid-state electrolyte has

1 a small polarization voltage in the symmetric cell. The Li/PUTP1/LFP solid-state battery at  
2 0.1C can not only achieve charge/discharge cycles at room temperature but also exhibits a better  
3 rate performance. This GPEs technique is expected to provide an opportunity for developing  
4 lithium metal batteries of high energy density and safe performance.

5



#### 1 4. Experimental Section/Methods

2 *Materials:* Poly(ethylene glycol) methyl ether methacrylate (PEGMA,  $M_n = 500 \text{ g mol}^{-1}$ ,  
3 98%, Aladdin), tripropylene glycol diacrylate (TPGDA, 99%, Aladdin), 1-Allyl-3-  
4 methylimidazolium Bis(trifluoromethanesulfonyl)imide (AMIMTFSI, 98%, TCI), 2-hydroxy-  
5 2-methylpropiophenone (97%, Aladdin), Bis(trifluoromethane)sulfonimide lithium salt  
6 (LiTFSI, >99%, Canrd),  $\text{LiFePO}_4$  (LFP, battery degree, Canrd), N-methyl-2-pyrrolidone (NMP)  
7 are analytically pure obtained by Sinopharm Chemical Reagent Co., Ltd.

8 *Synthesis of UPyMA:* UPyMA was synthesized using steps from the literature, with some  
9 modifications to the literature synthesis.<sup>[14]</sup> 6-methylisocytosine (10 g, 80 mmol), 2-  
10 isocyanatoethyl methacrylate (13.2 g, 85 mmol), and 150 ml DMSO solvent were added to a  
11 250 ml two mouth flask and heated to 150 °C until a pale yellow solution was formed. To  
12 acquire UPyMA monomer, the solution is allowed to stand for 12 hours before being filtered,  
13 rinsed three times with ethanol (50 ml), and dried at room temperature. The chemical reaction  
14 equation is shown in the diagram (Scheme S1, Supporting Information). The NMR hydrogen  
15 spectra showed that the UPyMA monomer was successfully prepared (Figure S26, Supporting  
16 Information).

17 *Synthesis of PUTP electrolyte:* The polymer electrolyte was prepared by a facile one-step  
18 photopolymerization. Taking PUTP1 as an example, UPyMA (0.084 g, 0.3 mmol), TPGDA  
19 (0.18 g, 0.6 mmol), PEGMA (1.5 g, 3 mmol), AMIMTFSI (1.5 g, 1 mol  $\text{kg}^{-1}$  LiTFSI solution),  
20 LiTFSI (0.407 g, with the EO/ $\text{Li}^+$  molar ratio of 16:1) and 2-hydroxy-2-methylpropiophenone  
21 (60 mg, 2 wt%) were dissolved in 4 mL DMSO. Then heated to 80 °C until the solution was  
22 completely clear and homogeneous. The above solution was then transferred to a Teflon mold  
23 and exposed to a UV light for 2h at a wavelength of 365 nm. Finally, the polymer film dried  
24 under vacuum overnight at 80 °C/-0.09 MPa and denoted as PUTP1. The samples of PUTP2

1 and PUTP3 were synthesized similarly to PUTP1, and the ratio of UPyMA to PEGMA is in  
2 Table 1. All samples were kept in the glove box ( $O_2 < 0.1$  ppm,  $H_2O < 0.1$  ppm) before testing.

3 *The ionic conductivity study:* The ionic conductivity was measured in the frequency range  
4 of 100 to  $10^6$  Hz by electrochemical impedance spectroscopy (EIS) with a potential static signal  
5 amplitude of 10 mV. The electrolyte was sandwiched between two stainless steel electrodes in  
6 a Swagelok cell, from 25 to 70 °C with an increment of 10 °C (Correst, China). The Swagelok  
7 cells assembled in the glove box ( $O_2 < 0.1$  ppm,  $H_2O < 0.1$  ppm) and the ionic conductivity  $\sigma$  can  
8 be evaluated by the following equation:

$$9 \quad \sigma = L/RS \quad (\text{Equation 1})$$

10 where  $R$ ,  $L$ , and  $S$  are the bulk resistance, thickness, and area of the solid-state electrolyte slice,  
11 respectively.

12 *Electrochemical stability assessment:* The electrochemical stability of the solid electrolyte  
13 was tested by the linear sweep voltammetry (LSV) technique. LSV was performed in the  
14 potential of 2.5-6 V *versus*  $Li^+/Li$  at 25 °C (scan rate 1 mV s<sup>-1</sup>) using a stainless  
15 steel/electrolyte/Li coin cells (CR2016), Li-metal diameter 14mm, PUTP diameter 18mm.

16 *Lithium-ion transference number:* The symmetric Li/PUTP/Li cells were assembled to  
17 determine  $Li^+$  transference number ( $t_{Li^+}$ ) using electrochemical impedance spectroscopy and  
18 chronoamperometry at 25 °C. The  $t_{Li^+}$  of electrolytes PUTP1, PUTP2, and PUTP3 were  
19 calculated by the Bruce-Vincent-Evans equation, a polarization voltage ( $\Delta V$ ) of 10 mV was  
20 applied to the symmetrical cells,  $I_0$  and  $I_s$  are the initial and steady-state current, while  $R_0$  and  
21  $R_s$  are the interfacial resistances at the initial and steady state, respectively.

$$22 \quad t_{Li^+} = \frac{I_s \Delta V - I_0 R_0}{I_0 \Delta V - I_s R_s} \quad (\text{Equation 2})$$

23 *Symmetric cell:* Li/PUTP/Li symmetric cell with constant current density plating/stripping  
24 at 0.05 mA cm<sup>-2</sup> and 0.1 mA cm<sup>-2</sup> respectively, with a plating/stripping cycle time of 0.5 h. The

1 diameter of the PUTP electrolyte is 18 mm and the diameter of the lithium metal is 8 mm.

2 *Preparation of cathode material:* By spreading the mixture of LFP, Super P and PVDF  
3 (initially dissolved in NMP) with a weight ratio of 8: 1: 1 onto an aluminum current collector  
4 the positive electrode was manufactured. Then dried at 60 °C at least 24 hours under ambient  
5 atmospheric pressure. Electrode sheet LFP with a load of 1.2-1.3 mg cm<sup>-2</sup>.

6 *Li battery assembly:* Coin cells (CR2016) were assembled with LFP cathode, Li metal  
7 anode and the solid-state electrolyte slices in a glove box filled with argon. Under a potential  
8 range of 2.0-4.0 V, the galvanostatic charge-discharge cycling output was reported on a LAND  
9 battery test device (CT2001A, LANHE, China). The charge and discharge current rates were  
10 fixed to C/10 at room temperature or C/5 at 25 °C.

## 11 **Supporting Information**

12 Supporting Information is available from the Wiley Online Library or from the author.

## 13 **Acknowledgements**

14 This work was supported by the National Natural Science Foundation of China (No. 21803040),  
15 Young Talent Support Plan of Xi'an Jiaotong University and the Engineering and Physical  
16 Sciences Research Council (EPSRC) grant-EP/N007921 and EP/S032886.

## 17 **Conflict of Interest**

18 The authors declare no conflict of interest.

19 Received: ((will be filled in by the editorial staff))

20 Revised: ((will be filled in by the editorial staff))

21 Published online: ((will be filled in by the editorial staff))

22

23

1 **References**

- 2 [1] a) Z. Chen, P.-C. Hsu, J. Lopez, Y. Li, J. W. F. To, N. Liu, C. Wang, Sean C. Andrews,  
3 J. Liu, Y. Cui, Z. Bao, *Nat. Energy*. **2016**, *1*, 15009; b) Q. S. Wang, P. Ping, X. J. Zhao,  
4 G. Q. Chu, J. H. Sun, C. H. Chen, *J. Power Sources*. **2012**, *208*, 210.
- 5 [2] a) Y. Xiao, Y. Wang, S.-H. Bo, J. C. Kim, L. J. Miara, G. Ceder, *Nat. Rev. Mater.* **2020**,  
6 *5*, 105; b) C. Wang, K. Fu, S. P. Kammampata, D. W. McOwen, A. J. Samson, L. Zhang,  
7 G. T. Hitz, A. M. Nolan, E. D. Wachsman, Y. Mo, V. Thangadurai, L. Hu, *Chem. Rev.*  
8 **2020**, *120*, 4257; c) T. Jiang, P. He, G. Wang, Y. Shen, C.-W. Nan, L.-Z. Fan, *Adv. Energy*  
9 *Mater.* **2020**, *10* 1903376; d) Q. Zhao, X. Liu, S. Stalin, K. Khan, L. A. Archer, *Nat.*  
10 *Energy*. **2019**, *4*, 365; e) J. Wan, J. Xie, X. Kong, Z. Liu, K. Liu, F. Shi, A. Pei, H. Chen,  
11 W. Chen, J. Chen, X. Zhang, L. Zong, J. Wang, L.-Q. Chen, J. Qin, Y. Cui, *Nat*  
12 *Nanotechnol.* **2019**, *14*, 705; f) M. Ebadi, T. Eriksson, P. Mandal, L. T. Costa, C. M.  
13 Araujo, J. Mindemark, D. Brandell, *Macromolecules*. **2020**, *53*, 764;
- 14 [3] D. Lin, Y. Liu, Y. Cui, *Nat Nanotechnol.* **2017**, *12*, 194.
- 15 [4] a) F. Guo, C. Wu, H. Chen, F. Zhong, X. Ai, H. Yang, J. Qian, *Energy Stor. Mater.* **2020**,  
16 *24*, 635; b) B. Li, Y. Wang, S. Yang, *Adv. Energy Mater.* **2018**, *8*, 1702296; c) X. Yang,  
17 J. Luo, X. Sun, *Chem. Soc. Rev.* **2020**, *49*, 2140; d) H. Liu, X.-B. Cheng, J.-Q. Huang,  
18 H. Yuan, Y. Lu, C. Yan, G.-L. Zhu, R. Xu, C.-Z. Zhao, L.-P. Hou, C. He, S. Kaskel, Q.  
19 Zhang, *Acs Energy Letters*. **2020**, *5*, 833; e) H. Zhang, G. Gebresilassie Eshetu, X. Judez,  
20 C. Li, L. M. Rodriguez-Martinez, M. Armand, *Angew. Chem. Int. Ed.* **2018**, *57*, 15002;  
21 f) Z. Li, J. Huang, B. Y. Liaw, V. Metzler, J. Zhang, *J. Power Sources*. **2014**, *254*, 168;  
22 g) D. Wang, W. Zhang, W. Zheng, X. Cui, T. Rojo, Q. Zhang, *Adv. Sci.* **2017**, *4*, 1600168.
- 23 [5] a) V. Bocharova, A. P. Sokolov, *Macromolecules*. **2020**, *53*, 4141; b) K. Wu, J. Huang,  
24 J. Yi, X. Liu, Y. Liu, Y. Wang, J. Zhang, Y. Xia, *Adv. Energy Mater.* **2020**, *10*, 1903977;  
25 c) D. Zhou, D. Shanmukaraj, A. Tkacheva, M. Armand, G. Wang, *Chem.* **2019**, *5*, 2326;  
26 d) K. S. Ngai, S. Ramesh, K. Ramesh, J. C. Juan, *Ionics*. **2016**, *22*, 1259.

- 1 [6] a) W. Liu, S. W. Lee, D. Lin, F. Shi, S. Wang, A. D. Sendek, Y. Cui, *Nat. Energy*. **2017**,  
2 2, 17035; b) I. Osada, H. de Vries, B. Scrosati, S. Passerini, *Angew. Chem. Int. Ed.* **2016**,  
3 55, 500; c) L. Long, S. Wang, M. Xiao, Y. Meng, *J. Mater. Chem. A*. **2016**, 4, 10038.
- 4 [7] a) Y. Li, Z. Sun, L. Shi, S. Lu, Z. Sun, Y. Shi, H. Wu, Y. Zhang, S. Ding, *Chem. Eng. J.*  
5 **2019**, 375, 121925; b) C. Wang, T. Wang, L. Wang, Z. Hu, Z. Cui, J. Li, S. Dong, X.  
6 Zhou, G. Cui, *Adv. Sci.* **2019**, 6, 1901036.
- 7 [8] G. Wang, X. Zhu, A. Rashid, Z. Hu, P. Sun, Q. Zhang, L. Zhang, *J. Mater. Chem. A*.  
8 2020, 8, 13351.
- 9 [9] Z. P. Wan, D. N. Lei, W. Yang, C. Liu, K. Shi, X. G. Hao, L. Shen, W. Lv, B. H. Li, Q.  
10 H. Yang, F. Y. Kang, Y. B. He, *Adv. Funct. Mater.* **2019**, 29, 1805301.
- 11 [10] R. Bouchet, S. Maria, R. Meziane, A. Aboulaich, L. Lienafa, J. P. Bonnet, T. N. Phan,  
12 D. Bertin, D. Gigmes, D. Devaux, R. Denoyel, M. Armand, *Nat. Mater.* **2013**, 12, 452.
- 13 [11] a) C. Cao, Y. Li, Y. Feng, P. Long, H. An, C. Qin, J. Han, S. Li, W. Feng, *J. Mater. Chem.*  
14 *A*. **2017**, 5, 22519; b) C. Cao, Y. Li, S. Chen, C. Peng, Z. Li, L. Tang, Y. Feng, W. Feng,  
15 *ACS Appl Mater Interfaces*. **2019**, 11, 35683; c) C. Cao, Y. Li, Y. Feng, C. Peng, Z. Li,  
16 W. Feng, *Energy Stor. Mater.* **2019**, 19, 401.
- 17 [12] B. Zhou, M. Yang, C. Zuo, G. Chen, D. He, X. Zhou, C. Liu, X. Xie, Z. Xue, *ACS Macro*  
18 *Letters*. **2020**, 9, 525.
- 19 [13] a) J. Hu, W. Wang, B. Zhou, Y. Feng, X. Xie, Z. Xue, *J. Membr. Sci.* **2019**, 575, 200; b)  
20 G. Jo, H. Jeon, M. J. Park, *ACS Macro Letters*. **2015**, 4, 225; c) H. Duan, Y.-X. Yin, X.-  
21 X. Zeng, J.-Y. Li, J.-L. Shi, Y. Shi, R. Wen, Y.-G. Guo, L.-J. Wan, *Energy Stor. Mater.*  
22 **2018**, 10, 85; d) W. Fan, N.-W. Li, X. Zhang, S. Zhao, R. Cao, Y. Yin, Y. Xing, J. Wang,  
23 Y.-G. Guo, C. Li, *Adv. Sci.* **2018**, 5, 1800559.
- 24 [14] B. Zhou, D. He, J. Hu, Y. Ye, H. Peng, X. Zhou, X. Xie, Z. Xue, *J. Mater. Chem. A*.  
25 **2018**, 6, 11725.

- 1 [15] a) J. Wan, J. Xie, X. Kong, Z. Liu, K. Liu, F. Shi, A. Pei, H. Chen, W. Chen, J. Chen,  
2 X. Zhang, L. Zong, J. Wang, L. Q. Chen, J. Qin, Y. Cui, *Nat Nanotechnol.* 2019, *14*, 705; b) T.  
3 Dong, J. Zhang, G. Xu, J. Chai, H. Du, L. Wang, H. Wen, X. Zang, A. Du, Q. Jia, X. Zhou, G.  
4 Cui, *Energy Environ. Sci.* 2018, *11*, 1197.
- 5 [16] a) Y. Li, Z. Sun, L. Shi, S. Lu, Z. Sun, Y. Shi, H. Wu, Y. Zhang, S. Ding, *Chem. Eng.*  
6 *J.* **2019**, *375*, 121925; b) X. Tian, P. Yang, Y. Yi, P. Liu, T. Wang, C. Shu, L. Qu, W. Tang, Y.  
7 Zhang, M. Li, B. Yang, *J. Power Sources.* **2020**, *450*, 121925.